

PANI Addition to Improve Contact Between CdTe/CdS Semiconductors

Paulo Herbert Franca Maia Junior^{a*} , Ana Fabiola Leite Almeida^a,

Raquele Lima Moreira^a, Edwalder Silva Teixeira^a , Vanja Fontenele Nunes^a ,

Diego Caitano Pinho^a, Francisco Nivaldo Aguiar Freire^a

^aUniversidade Federal do Ceará, Fortaleza, CE, Brasil.

Received: October 8, 2020; Revised: March 30, 2021; Accepted: April 27, 2021

This paper presents the study of the addition of the polyaniline polymer (PANI), at the junction of the cadmium telluride and cadmium sulfide (CdTe/CdS) layers in order to improve the contact between the layers, to decrease the air gap that limit the conversion photovoltaic. The morphology of CdS, CdTe and polyaniline (PANI) were characterized with multiple techniques including scanning electron microscopy (SEM), energy dispersive spectroscopy (EDS), X-ray diffraction (XRD) and optical absorption. The Metrohm Autolab LED Driver Kit system was used for data collection, and it was possible to obtain the current and voltage parameters of the cells. The inclusion of PANI thin film in CdS/CdTe hybrid solar cells increases the energy conversion efficiency from 0.0075% to 0.15%, this gives a 20-fold increase in efficiency.

Keywords: *Solar Cell CdS/CdTe, PANi.*

1. Introduction

In the last century, great discoveries were made by man, among them are fossil fuels, they are difficult to replace, however when verifying that these fuels are reaching the end of their extraction process, man seeks new ways to generate energy, in the middle of the last century, semiconductors were discovered and with them the necessary technology to generate electrical energy converted through sunlight.

The most well-known technology for converting solar energy into electricity is that of Silicon, due to its abundance on the planet, there are other materials that are more efficient, but they are difficult to find in nature, we can mention as an example: gallium, germanium and indium, among other metals and semi-metals. Another existing technology is that of Cadmium Telluride (CdTe), but the element tellurium in addition to being toxic is difficult to be found in nature and cadmium, despite being easier to be found in nature, is an extremely toxic metal.

With due technology, it is possible to make these cells more efficient and have a good level of safety. What is achieved nowadays¹.

There are several ways to transform solar energy into useful energy for humanity, one of these ways is to convert solar energy into electrical energy, using photovoltaic solar cells, so this is the reason for carrying out this work and the interest in contributing to the solution of the problem to the energy crisis, due to the high consumption of energy that only grows every year, as it is necessary to develop more and more systems that generate low-cost electricity². Solar CdS/CdTe cells have low manufacturing costs, but it is possible to improve their efficiency and this defines the objective

of this work. After extensive research in the literature, we can state that PANI has been used as a counter electrode and the proposal of this work is that PANI be placed in the middle of the solar cell, thus demonstrating the increase in its efficiency and a new use for PANI³.

2. Objective

- Synthesize CdS/CdTe solar cells.
- Synthesize and add the conducting polyaniline polymer (PANI) at the junction of the cells.
- Evaluate the efficiency of the cells by adding the PANI between the CdS/CdTe layers.

3. Materials and Methods

3.1. Preparation of deposition steps

Before all deposition processes, the FTO films were washed in an ultrasound bath for 30 min in a 1:1 solution of water and alcohol, being dried in an oven at 60 °C for 90 min, and finally stored in a desiccator, containing blue silica gel and remaining so until its use.

3.2. Deposition of CdTe

The materials available to prepare the precursor solution for CdTe are: tellurium oxide, sulfuric acid and cadmium chloride. Tellurium oxide, being an oxide, has a difficult solubilization in water, being solubilized in a 5 molar sulfuric acid solution, after verifying that all oxide was solubilized, a new dilution was made, lowering the solution concentration to 1 molar and an aqueous solution containing 1 molar cadmium chloride, the two solutions were then mixed using a magnetic

*e-mail: phfmj2010@gmail.com

stirrer and transferred to an electrochemical cell, whose assembly consists of reference electrode, against platinum electrode and working electrode (FTO film).

The reference electrode chosen was a calomel type electrode. To work as a counter electrode, a platinum plate with dimensions of 2 cm x 3 cm and thickness of 1 mm was chosen, the platinum was chosen because it is an inert metal. The working electrode was a thin FTO film, produced in the LAFFER laboratory (Thin Films and Renewable Energy Laboratory).

The CdTe was deposited by the electrodeposition method on a conductive glass of FTO, through a sequence of cyclic voltammetry, which consists of varying the voltage in the cell. After finishing the process, the films undergo a thermal treatment with a coating containing anhydrous CdCl₂ in methanol solution and this is taken to the vacuum oven for about an hour at 400 °C, temperatures above 490 °C favor the evaporation of the cadmium chloride, thus avoiding the deposition of excess cadmium on the substrate⁴, thus having the characteristic of being a semiconductor type p.

After the heat treatment, the film was washed using the ultrasound bath first with a solution containing methanol. Then the film is taken to the greenhouse for 24 hours at about 60 °C to remove all moisture and is subsequently stored in an airtight container containing blue silica gel and only leaving there to assemble the final device.

3.3. Deposition of CdS film

In another slide also containing the FTO film, the thin CdS film was deposited by chemical bath. Cadmium Chloride, Tiouréia and ammonia chloride, were diluted in deionized water in the concentration of 1 molar each, being put to heat to 80 °C according to the literature⁵. The Cadmium chloride solution was put in a Becker and at this moment the glasses containing the FTO are added, protected by an insulating mask so that only the unprotected part receives the CdS layer. The Ammonia and Cadmium chloride solutions were mixed and their pH was corrected to 10 using an NH₄OH solution, finally the solution containing thiourea was slowly dripped. The reaction does not occur instantly, it takes about 20 minutes until the whole process is finished. The baths were repeated and analyzed in UV-vis, then they were taken to the vacuum oven at 400 °C for 30 minutes. The films were then stored in a desiccator to avoid moisture.

3.4. Deposition of polyaniline films

Polyaniline was deposited by electropolymerizing the aniline monomer in an acid medium on the CdTe and CdS films, respectively. A solution containing 50 mL of 1 molar HCl was used as the base and 2 mL of the aniline was diluted with stirring, then a cyclic voltammetry was performed between -0.2 V and 1.2 V, starting and ending at 0 V, that is it can be considered a cycle, to have a notion of the thickness of the film, several samples were made with different cycles, 3, 6, 9 and 12 cycles respectively for each sample⁶. The resultant product was PANI in emeraldine salt form, i.e., PANI (ES). However, the more cycles are performed, the lower the transmittance making it difficult for photons to pass to the layer containing CdTe.

3.5. Characterization techniques

The structural, morphological, optical and electrical properties of PANI, CdTe and CdS films were characterized using X-ray diffraction, scanning electron microscopy, UV-VIS spectroscopy and photovoltaic characterization. The cell structures have the following characteristics: glass / FTO / CdS / PANI / CdTe / FTO / glass and were manufactured incorporating the PANI between the FTO/CdTe and FTO/CdS cells. The results show that with the addition of the polymer there is an improvement in the efficiency of the cells.

The characterizations were performed in the laboratories of the institution itself as the Central Analítica of the UFC, where the INSPECT S50 - FEI Electronic Scanning Microscope (SEM) was used, in the UFC X-Ray laboratory we have the Diffractometer for polycrystalline samples model XPert Pro MPD - Panalytical.

The absorbance and transmittance spectra were recorded using the Agilent Cary-300 spectrophotometer in the wavelength range 190-900 nm. The optical gap energy was calculated using Equations 1 and 2 through Tauc's plot method following the relationship.

$$(\alpha h\nu)^n = E(h\nu - E_g) \quad (1)$$

The Equation 1 is known as Tauc and Davis-Mott relation. This relation is used to probe the optical band gap energy of nanoparticles from UV-Vis absorption spectroscopy. In this equation, α is absorption coefficient, $h\nu$ is incident photon energy, E is energy independent constant and E_g in the optical band gap energy. In this equation the exponent "n" represents the nature of transition. For direct band gap material $n = 2$ while for indirect $n = 1/2$. We can calculate α from absorbance data using Beer Lambert's Law⁷.

$$E_g = h\nu \quad (2)$$

In Figure 1, I is the intensity of transmitted light, I_0 is the intensity of incident light, α is the absorbance coefficient and L is the path-length of light in which absorbance take place. According to Viezbicke the alpha coefficient has a value of 2.303.

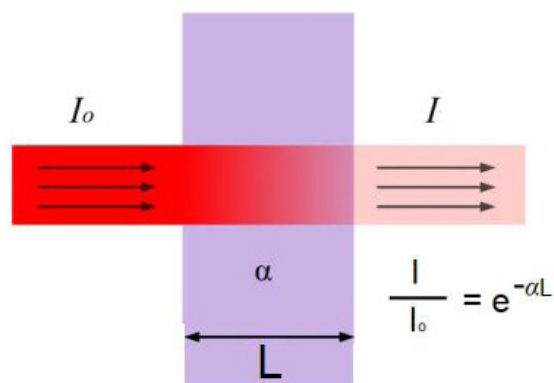


Figure 1. Beer Lambert Law. Source the author.

$$E = hv = \frac{hc}{\lambda} = \frac{1240}{\lambda} \quad (3) \text{ and}$$

$$(\alpha hv)^n = (2,303 * hv)^n \quad (4)$$

when plotting Equations 3 and 4 we will have the Tauc plot, where Equation 3 will be the energy for each wavelength on the x-axis and Equation 4 will be the absorbance coefficient plotted on the y-axis, this will then be the Tauc relationship, when we do $\alpha = 0$ at the point where you touch the x axis we will have the optical band gap, Equation 2⁷. The point where it touch the x-axis is the optical band gap energy of the material.

To characterize a Solar cell it is necessary to have an equipment that performs the measurements of the cell parameters, performed under standard conditions and international standard IEC 904-9⁸. The electrical parameters that characterize a Solar cell are: short circuit current (I_{cc}), open circuit voltage (V_{oc}), serial resistance (R_s), parallel resistance (R_p), load resistance (R_c), conversion efficiency (η) and form factor (FF). To determine these parameters the current intensity curve is used as a function of the potential difference applied; where (according to standard) the incident Irradiance must be 1000 W/m², the incidence spectrum is AM1.5G and the temperature 25 °C⁸. This curve thus obtained is known as the solar cell I-V curve. The solar cell has a structure similar to that of an ideal photodiode, it has a p-n junction structure, which when polarized, applying a voltage "V" - DC, in the dark, presents a characteristic I-V curve⁹.

The Potentiostat/Galvanostat PGSTAT302N, with the help of the Autolab LED Driver, was used to perform the cyclic voltammetry, electrodepositions and solar cell analysis. These were made in the UFC (LAFFER) thin film and renewable energy laboratory. The current density versus voltage (I-V) and characteristics of the solar cells were measured using the Autolab LED Driver kit 100 mW/cm² or 1000 W/m² the accessory works in a similar way to a solar simulator. The photoconversion efficiencies (PCE) of solar cell devices were obtained using the equations below.

$$\eta = \left(\frac{J_{sc} V_{oc} FF}{P_i} \right) \quad (5)$$

$$\text{where } FF = \left(\frac{P_{max}}{J_{sc} V_{oc}} \right) \quad (6)$$

J_{sc} is the short-circuit current density, V_{oc} is the open circuit voltage, FF is the form factor, P_{max} is the maximum power generated by the cell and P_i is the power incident on the cell. When applying Equation 6 in 5, we will have:

$$\eta = \frac{P_{max}}{P_i} \quad (7)$$

4. Results and Discussions

X-ray diffraction is a technique used to determine the atomic and molecular structure of a crystal, in which the crystalline atoms cause a beam of incident X-rays to diffract in many specific directions.

By measuring the angles and intensities of diffracted beams, a crystallograph can produce a three-dimensional image of the density of electrons within the crystal. From this electron density, the average positions of the atoms in the crystal can be determined, as well as their chemical bonds, their disorder and various other information¹⁰, Figures 2 and 3 show the diffractory films of CdTe and CdS, deposited by electrodeposition and chemical bath techniques respectively, on thin FTO film.

In Figure 2 the presence of CdS and FTO peaks were observed, according to the JOINT COMMITTEE FOR POWDER DIFFREACTON STANDARDS database (JCPDS-10-0454 for CdS and JCPDS-77-450 for FTO)¹¹. After the determination of phases, Miller's indexes were determined by comparison with JCPDS standards, thus concluding that the deposited film has preferential orientation and growth in the plan (111). The other plans (200) and (311) were also observed in the literature¹¹ and correspond to the cubic phase of the CdS. The X-ray diffraction serves as a system for identifying materials, because each atomic set has crystallographic characteristics that are unique, so we can state that the synthesized material is indeed the one planned¹².

The X-ray diffraction patterns of the annealed film are shown in Figure 2. Three major diffraction peaks are appearing at 2 θ ~26.6°, 43.98° and 52.23° which are assigned to the

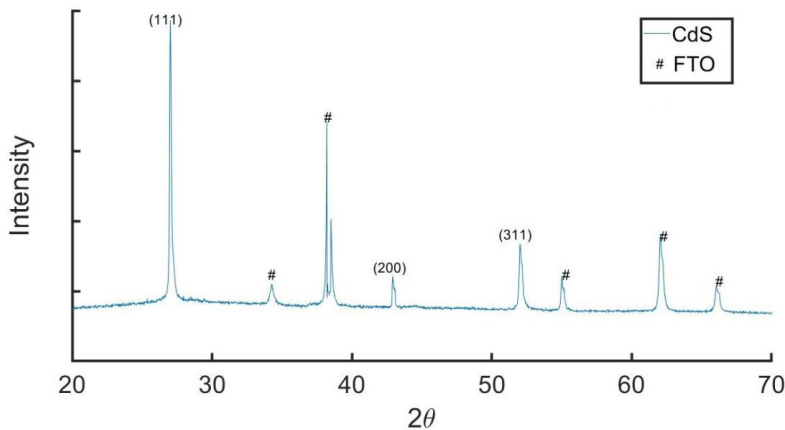


Figure 2. Difractogram of the CdS film on FTO substrate. Source the author.

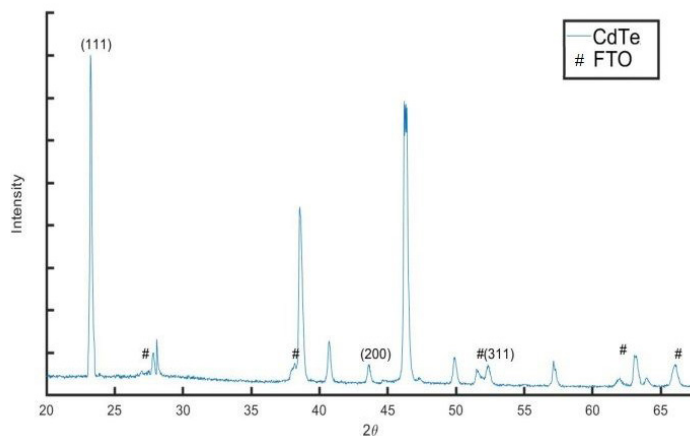


Figure 3. CdTe film diffractory on FTO substrate. Source the author.

(111), (200) and (311) reflections of cubic CdS. The X-ray diffraction profiles clearly shown that the intensity of the (111) peak is higher than other crystalline phases. The diffraction patterns of the films are found to be matched well with the JCPDS card No. 10-0454. The intense diffraction peak appearing approximately at $2\theta = 26.6^\circ$ corresponds to the (111) plane of the cubic CdS¹³. The width at half height of the peaks is related to the size of their crystals according to Scherrer's equation.

$$D = \frac{K\lambda}{\beta \cos\theta} \quad (8)$$

Where D is the Crystallite size in nm, K is 0.9 (Scherrer constant), λ is 0.15406 nm (wavelength of the x-ray source), θ is peak position (radians) and β is the half height of the FWHM peak (radians). The CdS deposited by chemical bath presents size of its small crystals as shown in Table 1, probably did not achieve greater ordering or growth by the low temperature used in chemical bath process which was 80 °C. The CdS deposited on the conductive oxide is strongly influenced by this material, presenting peaks in the same positions as the FTO, probably due to the structural and chemical affinity of these materials, as a consequence we have a greater adherence between them¹³.

In Figure 3 the presence of CdTe peaks were observed according to the JCPDS-10-0207 database, which corresponds to the cubic phase of the CdTe¹². The CdTe showed a higher intensity peak in the plane (111) demonstrating the possible preferential growth in this position, the other planes 200 and 311 were also observed in the literature affirming the cubic phase of the CdTe. The FTO substrate showed peaks in the planes (102), (200), (210), (310) and (301), by comparison with the crystallographic chart JCPDS-77-450¹⁴. By comparison between the peaks found and those of the crystallographic chart, we can affirm that, the synthesized material is in fact the CdTe and FTO, respectively. The CdTe deposited by electrodeposition presents the size of its small crystals as shown in Table 2, probably did not achieve greater ordering or growth by the low temperature used in the electrodeposition process room temperature.

Comparing Figure 4a with Figure 5a, we can clearly see that in the visible region the CdS has an average absorbance

Table 1. Average size of CdS cristals on FTO substrate per CBD.

Peak position 2θ	(FWHM)	Crystallite size (nm)
27,03217	0,17401	46,9546493
42,96311	0,20815	41,0152791
52,06451	0,1193	74,1094747
Average Size		54,0265

Table 2. Average CdTe/FTO cristalits size by electrodeposition.

Peak position 2θ	(FWHM)	Crystallite size (nm)
23,22	0,22862	35,47468743
43	0,33956	25,14551926
52,36	0,17403	50,8673174
Average Size		37,16250803

of 25%, while the CdTe has an absorption range that varies from 60 to 85%. We also calculated the GAP energies using the Tauc plot method, as described in Equation 4, where we found a bandgap of 2.34 eV for the CdS¹⁵ and 1.43 eV for the CdTe, Figure 4b and Figure 5b¹⁶.

For the CdTe deposition, potentials were chosen according to the analysis of the voltamogram obtained at a scanning speed of 50mV.s⁻¹, as shown in Figure 6, which suggests different phases of the electrodeposition process, highlighted in Figure 7, the phase **a** is the potential where the beginning of the nucleation process and thin film growth is occurring, phase **b** is the potential where the activation and diffusion control phases are operative, phase **c** is the cathode current peak potential where the deposition of Te occurs and phase **d** is the cathode current peak potential where the deposition of Cd occurs, phase **e** is the current threshold potential that closes the deposition process¹⁴.

The polyaniline films were electrodeposited on the CdS and CdTe films after they had undergone a heat treatment. The PANI deposits were made on a clean substrate containing only FTO in order to study material transmittance through UV-Vis. With this information we can calculate the bandgap of the material and know how much energy is passing through to the back of the cell. This can be seen from Figure 8, where with only 3 layers in the visible region the transmittance is between 70 and 80% and when the number of layers was increased to 8 the transmittance was below 20% in the visible

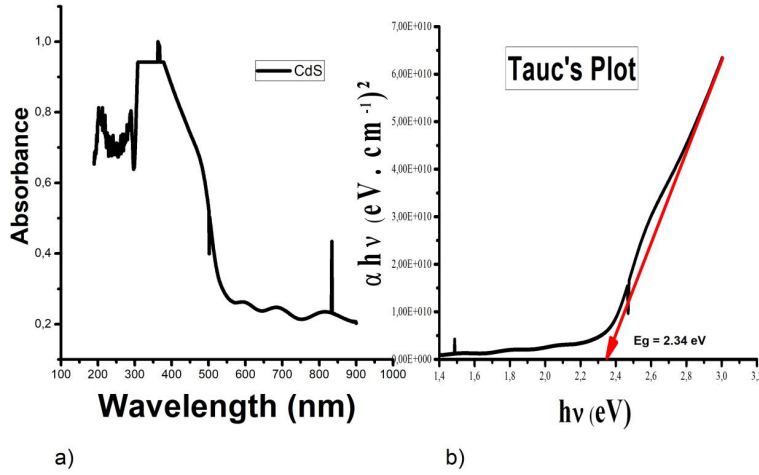


Figure 4. a) CdS Absorbance and b) Band Gap Graph. Source: the author.

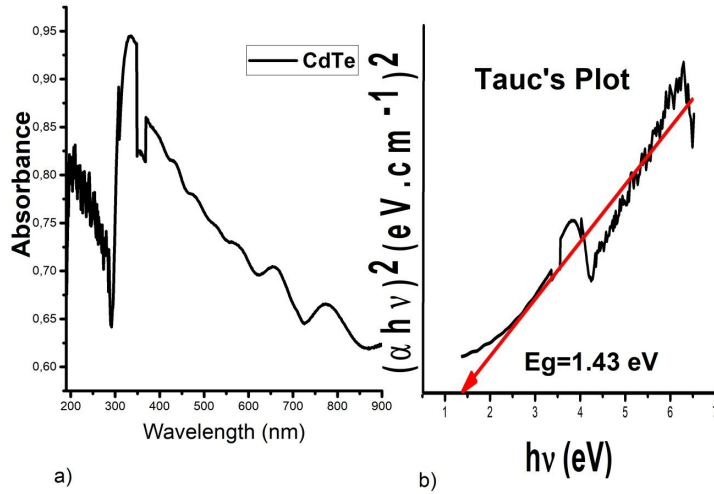


Figure 5. a) CdTe Absorbance and b) Band Gap Graph. Source: the author.

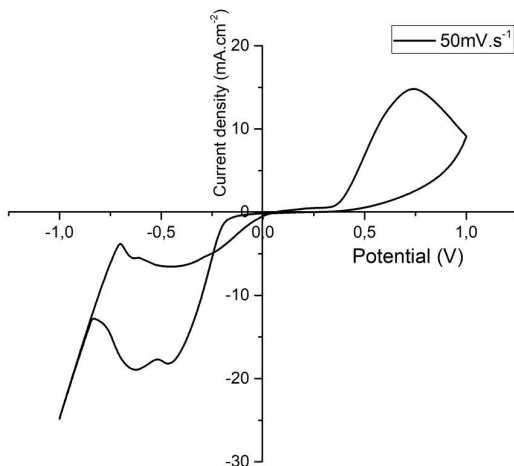


Figure 6. CdTe cyclic voltammetry graph at 50 mV/s⁻¹ scan speed. Source: the author.

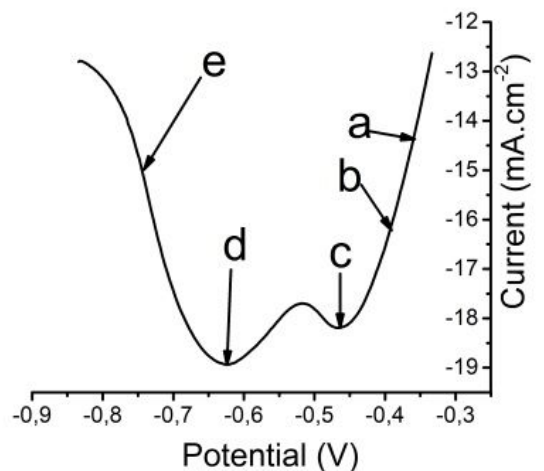


Figure 7. Description of the electrodeposition phases of the CdTe. Source: the author.

region which indicates that the number of layers influences the amount of photons that will cross to the CdTe layer¹⁷.

Figure 9a show SEM images with increased of 50000x, it is possible verify a sample with a good deposition, since the grains found in the surfaces are evenly spread. The micrographs obtained showed the distribution of the selective surface on the FTO substrate after the heat treatment, following the composition presented in Table 3.

Figure 9b shows how the concentration of a given element varies over an area of the sample, we can state that the distribution is uniformly distributed. The graph of Figure 9c indicates through the intensity of the Energy peaks of EDS,

Table 3. CdTe Film composition.

Element	Weight (%)
Te	53,4
Cd	43,4
Cl	3,1
Sn	0,1

Table 4. CdS Film composition.

Element	Weight (%)
Cd	16,2
S	4,9
Cl	0,6
Sn	36,4
Ca	2,0
Na	0,7
O	4,9
Si	10,1

Table 5. Parameters of CdS/CdTe cells.

Cell without PANI							
Isc (mA/cm ²)	Voc (V)	Imax (mA)	Vmax (V)	FF	Rsh (Ω)	Rs (Ω)	η (%)
0,025	0,39	0,0148	0,25	0,32	54,4	0,1	0,0075
Cell with PANI							
Isc (mA/cm ²)	Voc (V)	Imax (mA)	Vmax (V)	FF	Rsh (Ω)	Rs (Ω)	η (%)
0,35	0,67	0,17	0,43	0,37	7,7	0,71	0,153

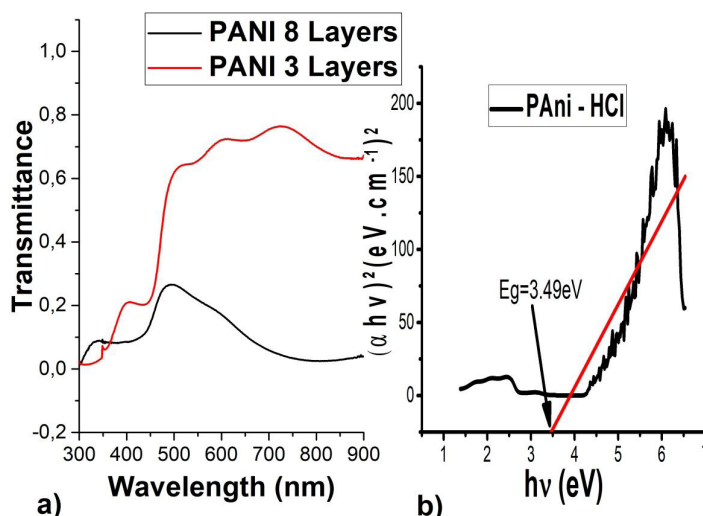


Figure 8. Transmittance graph and Bandgap graph of PANI. Source: the author.

the presence of Cd and Te, among others that are present in the sample, we observe that the amount of cadmium and tellurium are approximately 1:1, since we have 53.4% of Te and 43.4% of Cd, therefore we have actually: Cd_{0.8}Te. As can be observed through Table 3, there is the presence of chlorine and tin, and these, are due to the acid nature of the preparation solution and the thin film of FTO present in the substrate.

The Figure 10a shows the MEV of the CdS with 20000x magnification and its composition map in Figure 10b. In the graph of Figure 10c, we have the distribution of the amounts of cadmium and sulfur in percentage, the amount of sulfur in relation to cadmium is three times smaller having thus a ratio of 3:1, following the composition presented in Table 4. There is also the presence of other elements such as silicon, calcium and sodium, these are constituents of the composition of the glass substrate.

Figures 11 and 12 show the current density versus voltage graphs, without and with polyaniline and their respective electrical characteristics, it can be seen from Figure 11 that without polyaniline the open circuit voltage is less than 0.4 V, the current density is 0.025 mA/cm² and with efficiency of 0.007%. However when adding PANI the same cell had its characteristics altered as Figure 12, its open circuit voltage increased to 0.67 V, its current density increased to 0.3 mA/cm² and its efficiency was increased to 0.15%. The Rs had an increase, probably due to the fact that the resistance of the PANI is higher, which causes a zone of higher resistance the passage of electrons between the layers. The Rsh decreased due to the loss of current at the ends, caused by contact between the FTO film and the measuring apparatus. The parameters of the cells without and with PANI can be observed through Table 5.

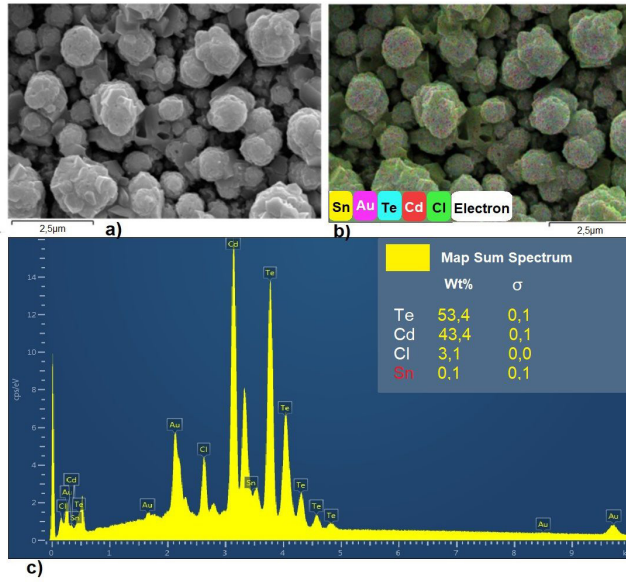


Figure 9. a) Micrograph of the surface sample of CdTe, with magnification factor of 50000x, b) composition map and c) EDS of the sample of CdTe. Source: the author.

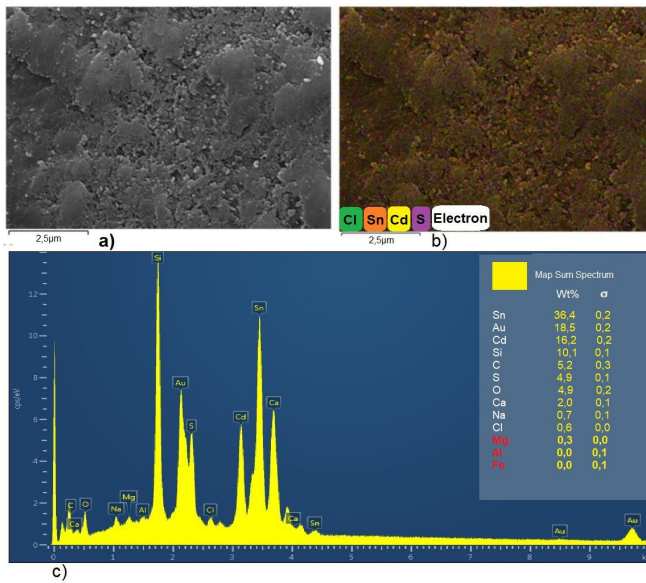


Figure 10. a) Micrograph of the surface sample of CdS, with magnification factor of 20000x, b) composition map and c) EDS of the sample of CdS. Source: the author.

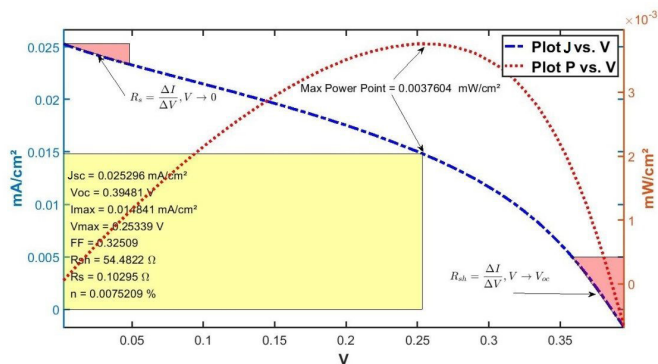


Figure 11. I – V curves for CdS / CdTe solar cells without addition of PANI. Source: the author.

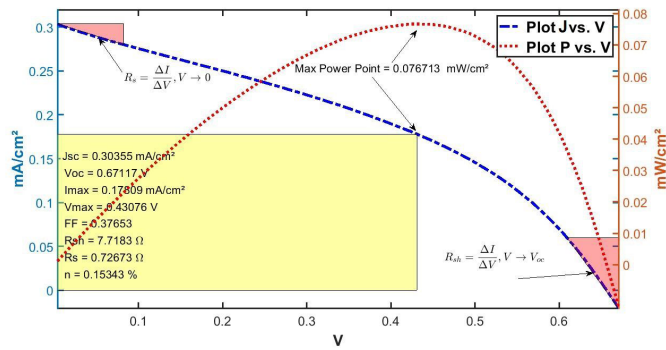


Figure 12. I – V curves for CdS / CdTe solar cells with addition of PANI. Source: the author.

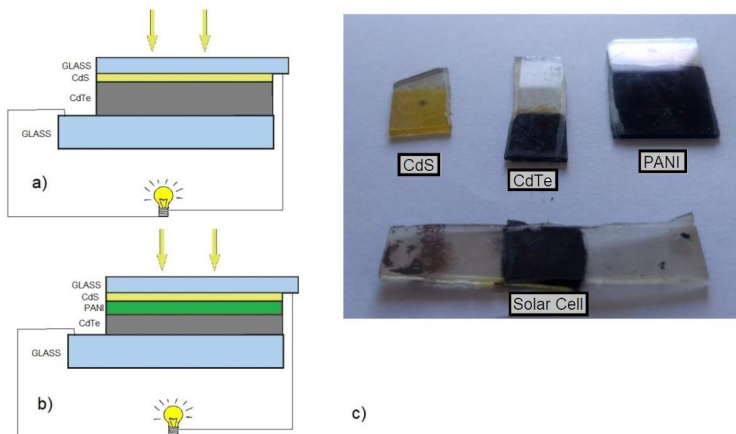


Figure 13. a) Assembly diagram of the cell without PANI, b) assembly diagram with PANI and c) the parts of the cell and its assembly. source: the author.

The dashed line in blue represents the relationship between current density (mA/cm^2) versus voltage (V), the dotted line in red represents the power density curve (mW/cm^2) versus voltage (V), the chart in yellow represents the fill factor and within it are the main properties of the cells, this graph was generated from an algorithm written in MatLab by the author himself.

Figure 13a shows the assembly diagram of the cell without PANI and Figure 13b with PANI. In Figure 13c we have the separate parts of the cell without PANI and the cell assembled with PANI between the junction, to improve the contact between the extremities silver paint was used before the photovoltaic characterization.

5. Conclusion

The addition of PANI to the CdTe/CdS system demonstrated that it is possible to incorporate the polymer between layers by the electroplating technique and that it improves the contacts between the CdS and CdTe layers, as shown in Figure 12, thus increasing the efficiency of the cell by 20 times. However, the resistances in series and in parallel also showed values outside the standard. The R_s should ideally have the value of zero and the R_{sh} should be infinite, as in the diode, this did not occur due to the short circuits promoted by the type of sealing of the cell, because it was only deposited and overlapped, without any type of

blockage or barrier that avoided the escape of electrons, because the aim was to highlight the increase in efficiency with the use of PANI between the layers of semiconductors type n (CdS) and type p (CdTe). We have proven that the use of PANI in a different position than usual in the solar cell (since no similar work was found in the literature), increases the voltage, the current, and therefore the efficiency of the cell, due to the increased contact between the layers.

6. Acknowledgements

The authors wish to thank Prof. Francisco Nivaldo Aguiar Freire of the Federal University of Ceará (UFC-Ce), for his orientation, support and for giving up his laboratory for research. Additional thanks are given to Coordination for the Improvement of Higher Level Personnel (CAPES) and the National Council for Scientific and Technological Development (CNPQ) for financial support and for the Post-GRADUATE ENGINEERING AND SCIENCE OF MATERIALS program (PPGECMAT).

7. References

- Galindo MAE, Lima JHG, Ribeiro CM, Serra ET. O contexto das energias renováveis no Brasil. Revista da Direng - CEPEL. 2009:17-25.
- Morales OM. Construção e caracterização de células solares de filmes finos de CdS e CdTe [dissertação]. Ilha Solteira:

- Universidade Estadual Paulista “Júlio de Mesquita Filho”; 2011.
- Alkum E, Mohammed M, Chen TP. Fabrication of CdS nanorods and nanoparticles with PANI for (DSSCs) dye-sensitized solar cells. *Sol Energy*. 2017;150:317-24.
 - Falcão VD. Fabricação de células solares de Cds/CdTe [dissertação]. Rio de Janeiro: Instituto Militar de Engenharia - IME; 2005.
 - Han J, Spanheimer C, Haindl G, Fu G, Krishnakumar V, Schaffner J, et al. Optimized chemical bath deposited CdS layers for the improvement of CdTe solar cells. *Sol Energy Mater Sol Cells*. 2011;95(3):816-20.
 - Li Z, Ye B, Hu X, Ma X, Zhang X, Deng Y. Facile electropolymerized-PANI as counter electrode for low cost dye-sensitized solar cell. *Electrochem Commun*. 11(9):1768-71.
 - Viezbicke BD, Patel S, Davis BE, Birnie DP 3rd. Evaluation of the tauc method for optical absorption edge determination: ZnO thin films as a model system. *Phys Status Solidi, B Basic Res*. 2015;252(8):1700-10.
 - Eberhardt D. Desenvolvimento de um sistema completo para caracterização de células solares [tese]. Porto Alegre: Faculdade Engenharia, Pontifícia Universidade Católica do Rio Grande do Sul; 2005.
 - Silva R, Chiquito AJ, de Souza MG, Macedo RP. Células solares “caseiras”. *Revista Brasileira de Ensino de Física* [serial on the Internet]. 2004 [cited 2018 Aug 20];26(4):379-4. Available from: <http://www.sbfisica.org.br/rbef/pdf/040608.pdf>
 - Andrade ENC. The principles of X-ray diffraction. London: International Union of Crystallography; 1999.
 - Manikandan K, Dillip CS, Mani P, Joseph Prince J. Deposition and characterization of CdS nano thin film with complexing agent triethanolamine. *Am J Eng Appl Sci*. 2015;8(3):318-27.
 - Marandi M, Mirahmadi FS. Aqueous synthesis of CdTe-CdS core shell nanocrystals and effect of shell formation process on the efficiency of quantum dot sensitized solar cells. *Sol Energy*. 2019;188:35-44.
 - Senthamilselvi V, Ravichandran K, Saravanakumar K. Influence of immersion cycles on the stoichiometry of CdS films deposited by SILAR technique. *J Phys Chem Solids*. 2013;74(1):65-9.
 - Sousa JHA, Maia PHF Jr, Silva ÁNA, Lima FM, Oliveira FWC, Magalhães RA, et al. Caracterização da eletrodeposição de filmes finos de CdTe sobre Pt em meio ácido. *Matéria (Rio J)*. 2015;20(4):866-81.
 - Lisco F, Kaminski PM, Abbas A, Bowers JW, Claudio G, Losurdo M, Walls JM. High rate deposition of thin film cadmium sulphide by pulsed direct current magnetron sputtering. *Thin Solid Films*. 574:43-51.
 - Ming Z, Ding C, Li B, Feng L. Study of Ar + O₂ deposition pressures on properties of pulsed laser deposited CdTe thin films at high substrate temperature. *J Mater Sci Mater Electron*. 2015;25(4):1901-7.
 - Ninh DH, Thao T, Long PD, Dinh NN. Characterization of electrochromic properties of polyaniline thin films electropolymerized in H₂SO₄ solution. *Open J Org Polym Mater*. 2016;6(1):30-37.